"Plastic Deformation" Mechanism and Phase Transformation in a Shear-Induced Metastable Hexagonally Perforated Layer Phase of a Polystyrene-*b*-poly(ethylene oxide) Diblock Copolymer

Lei Zhu,*,# Ping Huang,† William Y. Chen,† Xin Weng,† Stephen Z. D. Cheng,*,† Qing Ge,† Roderic P. Quirk,† Tony Senador,# Montgomery T. Shaw,# Edwin L. Thomas,‡ Bernard Lotz,§ Benjamin S. Hsiao,⊥ Fengji Yeh,⊥ and Lizhi Liu⊥

Maurice Morton Institute and Department of Polymer Science, The University of Akron, Akron, Ohio 44325-3909; Polymer Program, Institute of Materials Science and Department of Chemical Engineering, The University of Connecticut, Storrs, Connecticut 06269-3136; Department of Materials Science and Engineering, Massachusetts Institute of Technology, Cambridge, Massachusetts 02139; Institute Charles Sadron, 6 Rue Boussingault, Strasbourg 67083, France; and Department of Chemistry, The State University of New York at Stony Brook, Stony Brook, New York 11794

Received November 27, 2002; Revised Manuscript Received February 28, 2003

ABSTRACT: The hexagonally perforated layer (HPL) phase in a polystyrene-*b*-poly(ethylene oxide) (PS-*b*-PEO) diblock copolymer was systematically studied by small-angle X-ray scattering (SAXS) in reciprocal space and transmission electron microscopy (TEM) in real space. Detailed crystallographic analyses revealed that the shear-induced, "single-crystal"-like HPL phase in the PS-*b*-PEO diblock copolymer sample contained a mixture of trigonal twins (∼80%) and hexagonal (∼20%) structures. Both structures had the same orientation and the same in-plane unit cell parameters (*a* and α) but different out-of-plane (*c*-axis) dimensions, because the trigonal structure was constructed by three layers (ABC) and the hexagonal structure had two layers (AB). Computer-simulated diffraction and TEM results implied that the correlation length of the trigonal structure along the [001] direction was relatively large (at least over 20 layers, i.e., ≥∼400 nm) while that of the hexagonal structure was relatively small. The formation mechanism of the HPL phase was investigated by TEM. Various edge dislocations formed by "plastic deformation" under a large-amplitude mechanical shear were the cause of the trigonal twins and the hexagonal structure. Low-frequency rheological studies indicated that the HPL phase was metastable, and it transformed into a more stable double gyroid phase when the temperature exceeded 160 °C. The HPL structure reappeared after the sample was again subjected to the large-amplitude mechanical shear. Furthermore, the transformation from the HPL phase to the DG phase was also studied. It was found that the perforations of the hexagonal structure rearranged themselves first, followed by the perforations in the trigonal structure.

Introduction

Over the past few decades, ordered nanostructures have been produced from the self-assembly of block copolymers due to the incompatibility of chemically distinctive blocks that are covalently bonded to one another at their chain ends.[1,2] In addition to three conventional phase structures for diblock copolymers, i.e., lamellae, hexagonal cylinders, and body-centered-cubic spheres (bcc), complex phases have also been observed such as double gyroid (DG) and hexagonally perforated layers (HPL). The DG phase (space group $Ia\bar{3}d$),[3,4] first identified in solid soaps,[5] is a bicontinuous cubic phase. Its structure consists of channels of the minority component, linked three by three, forming two interwoven three-dimensional (3D) networks. Theoretical calculations have suggested that the DG phase is an equilibrium phase structure in the weak-to-intermediate segregation limit.[6,7] The perforated layer phase was first proposed to be a lamellar−catenoid structure in which both components were three-dimensionally connected.[8] This structure was then observed experimentally in diblock copolymer/homopolymer blends.[9,10] On the basis of the results of combined small-angle neutron scattering (SANS) and transmission electron microscopy (TEM) experiments, a shear-induced perforated lamellar structure in a poly(ethylene-*alt*-propylene)-*b*-poly(ethylethylene) (PEP-*b*-PEE) diblock copolymer was identified.[11,12] A monocontinuous morphology was proposed consisting of alternating minor and major component layers. Within the minority layers, the perforations of the major component had a hexagonal arrangement and were staggered between adjacent layers.

Since these observations, the stacking sequence of the hexagonal perforations in the HPL phase has received much attention. The stacking sequences may be modeled as ABC and/or AB arrangements. The ABC stacking is a trigonal (rhombohedral) structure (space group $R3m$), and the AB stacking is a hexagonal structure (space group $P6_3/mmc$) as shown in Figure 1. In special cases, if both are close-packed, the ABC and AB stackings become face-centered-cubic (fcc) and hexagonally close-packed (hcp) phases, respectively. From the two-dimensional (2D) SANS study on the shear-oriented HPL phase in a PEP-*b*-PEE sample, the AB stacking was considered to be favored locally, and it resembled the hexatic phase of thermotropic liquid crystals.[12]

† The University of Akron.
# The University of Connecticut.
‡ Massachusetts Institute of Technology.
§ Institute Charles Sadron.
⊥ The State University of New York at Stony Brook.
* To whom correspondence should be addressed. E-mail scheng@uakron.edu and lei.zhu@uconn.edu.

10.1021/ma021718x CCC: $25.00
Published on Web 04/03/2003

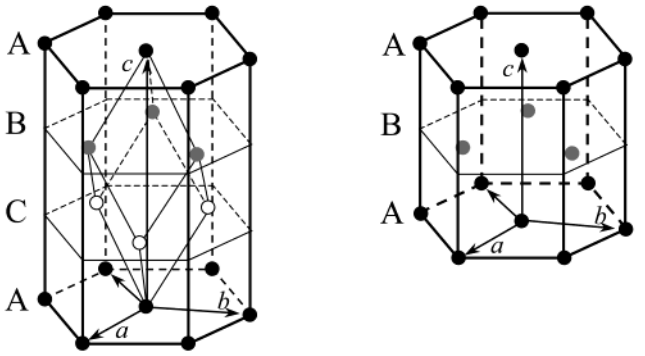

Figure 1. Schematic representation of the trigonal ABC (a) and hexagonal AB (b) stacking sequences. The two structures have the same *a* and α unit cell parameters, but the *c*-axis of the trigonal structure is $^3/_2$ times of that of the hexagonal structure. The trigonal primitive cell is also shown in (a).

Later, the fcc ABC stacking was proposed on the basis of a 2D SANS study of the sheared HPL phase in a polyisoprene-*b*-polystyrene (PI-*b*-PS) diblock copolymer.[13] Recently, an ordered HPL phase in a PEE-*b*-poly(dimethylsiloxane) diblock copolymer was observed using a synchrotron small-angle X-ray scattering (SAXS) technique. The 2D SAXS pattern of the oriented HPL phase was deduced on the basis of a combination of the fcc ABC stacking and hcp AB stacking.[14] The shear-induced HPL phase in a PI-*b*-PS diblock copolymer was also studied using synchrotron SAXS. A pure trigonal ABC stacking sequence was proposed on the basis of a [00*l*] uniaxial pattern of the HPL phase.[15]

Theoretical calculations of the HPL structure were carried out using a broad range of symmetry assumptions to predict the stability of the shear-induced HPL phase[16−24] such as catenoid−lamellar, fcc (ABC), hcp (AB), trigonal $R\bar{3}m$ (ABC), and bcc. Different thermodynamic stabilities of the HPL phase were obtained on the basis of these theoretical structural assumptions. Recent experimental findings have suggested that the HPL phase was induced by mechanical shear, and it was a long-lived metastable phase or intermediate state.[25]

In a most recent report, the HPL phase was observed in a polystyrene-*b*-poly(ethylene oxide) (PS-*b*-PEO) diblock copolymer with the volume fraction of 0.39 for the PEO block.[26] Synchrotron 2D SAXS study on the macroscopically oriented diblock copolymer "single crystals" along the *x*, *y*, and *z* directions (see Figure 2) demonstrated that the HPL phase possessed mixed structures with a majority of trigonal twins (ABC and ACB) and a minority hexagonal (AB) structure. The TEM results along the *x*-axis showed that the formation mechanism of the HPL phase was attributed to the "plastic deformation" (various edge dislocations) under a large-amplitude mechanical shear.

In this paper, we provide further evidence on the SAXS crystallographic analyses using tilted patterns obtained from different zones of the HPL phase to quantitatively describe the mixed structures. TEM results in real space along the [120] and [001] zones were also investigated. Computer-simulated diffractions provided more information on how the trigonal twins mixed with the hexagonal structure and information about the correlation lengths of the trigonal and hexagonal grains in the layer normal (the [001]) direction.

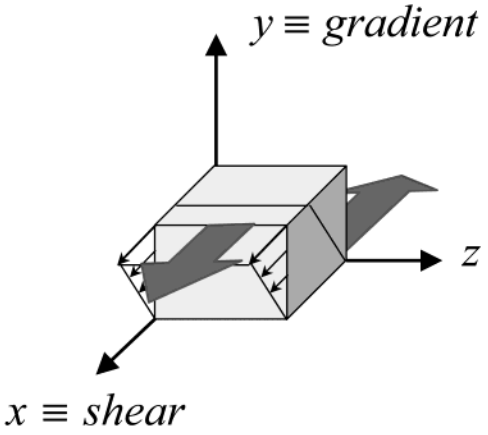

Figure 2. Shear geometry for the PS-*b*-PEO diblock copolymer samples.

The relative population of trigonal twins and hexagonal structures was evaluated on the basis of the reflection intensity ratio between the (011) reflection of the trigonal structure and the (010) of the hexagonal structure in the SAXS pattern. The metastability of the HPL phase was investigated using low-frequency, oscillatory shear rheological measurements. The phase transformation process from the HPL phase to the DG phase was also investigated.

Experimental Section

Materials and Sample Preparation. The synthesis and purification procedures of the PS-*b*-PEO diblock copolymers were described previously.[27] The PS block had a number-average molecular weight ($\bar{M}_n$) of 17k g/mol and a polydispersity of 1.02 as characterized by size exclusion chromatography (SEC) using PS standards. The $\bar{M}_n$ of the PEO blocks was 11k g/mol as determined by proton nuclear magnetic resonance (^{1}H NMR). The polydispersity of the final diblock copolymer was 1.09 using SEC with a universal calibration. The volume fraction of PEO blocks was 0.39. The glass transition temperature of the PS blocks (T_g^{PS}) and the melting temperature of the PEO blocks (T_m^{PEO}) were 72 and ∼51 °C, respectively, based on differential scanning calorimetry measurements. The order-to-disorder transition temperature (T_{ODT}) was ∼210 °C as identified by both temperature-dependent SAXS and low-frequency rheological experiments. The Flory−Huggins interaction parameter (χ) between the styrene (St) and ethylene oxide (EO) monomers was determined to be $\chi_{St/EO} = -0.00705 + 21.3/T$.[27] Therefore, the χN (N is overall degree of polymerization) value at 50 °C was approximately 24.7, which suggests that the PS-*b*-PEO diblock copolymer was in the weak-to-intermediate segregation limit. In the calculation of χ, the molar volumes for styrene and ethylene oxide segments were 98.73 and 39.25 mL/mol.[27]

The samples were cast from 5% (w/v) toluene solutions, and the solvent was allowed to evaporate under a dry nitrogen atmosphere at 50 °C over 3 days. Residual solvent was removed under vacuum at 50 °C for another 2 days, and the sample was then annealed at 100 °C for 12 h to allow microphase separation. The microphase-separated samples were then subjected to a large-amplitude reciprocating shear under a dry argon atmosphere at 120 °C to achieve uniform alignment of the microdomains on a macroscopic scale. The shear frequency was 0.5 Hz, and the shear amplitude was 150%. The shear direction was along the *x* direction, and the shear gradient was along the *y* direction, as shown in Figure 2. The shear plane was the *xz* plane. The sample was removed from the shear apparatus and quenched to room temperature. The sample dimensions were approximately 1 × 1 × 0.2 mm.

Equipment and Experiments. 2D SAXS experiments were conducted on the synchrotron X-ray beamline X27C at the National Synchrotron Light Source in Brookhaven Na-

tional Laboratory. The wavelength of the X-ray beam was 0.1307 nm. The zero pixel of the 2D SAXS pattern was calibrated using silver behenate, with the first-order scattering vector q ($q = 4\pi \sin\theta/\lambda$, where λ is the wavelength and 2θ the scattering angle) being 1.076 nm^{-1}. The air scattering was subtracted. The X-ray beam spot dimension was 0.1 mm in diameter. All the experiments were conducted at room temperature, since the PS layers and perforations became glassy below T_g^{PS} and preserved. The X-ray beam was not only aligned parallel to the *x*, *y*, and *z* directions (see Figure 2) but also along the axes obtained by rotating the *x* or *z* direction. To understand the transformation mechanism of the HPL phase toward the DG phase, the sample was heated to five temperatures between 120 and 160 °C, which were below the T_{ODT} but higher than both T_m^{PEO} and T_g^{PS}. At each temperature, the sample was held for 15 min before quenching to room temperature for the 2D SAXS patterns along the *x*, *y*, and *z* directions.

Cerius2 version 4.6 was used to carry out computer-simulated diffractions for the diblock copolymer structures. Instead of constructing the complex PS-*b*-PEO trigonal and hexagonal structures, Ar atoms arranged in both ABC and AB stackings were used to represent the desired structures as an approximation.

Rheological experiments were performed on an Advanced Rheometric Expansion System (ARES) dynamic mechanical spectrometer. First, a copolymer film with a thickness of ~0.5 mm was placed between a pair of parallel plates with a diameter of 10 mm. The samples were subjected to a 100% amplitude/1 rad/s frequency shear at 100 °C for 30 min to generate the HPL phase. Then they were then heated in the rheometer from 100 to 200 °C with N_2 protection at a rate of 2 °C/min. A 1% strain and 0.5 rad/s oscillation frequency were subsequently used to measure the shear storage modulus (G') change with temperature.

TEM experiments were carried out at an accelerating voltage of 120 kV on a JEOL 1200 EX II. Thin slices for TEM experiments were obtained using a Reichert Ultracut S (Leica) ultra-cryomicrotome to section the shear-aligned samples along the *x*, *y*, and *z* directions (see Figure 2). The sample was stained under RuO_4 vapor for 20 min at room temperature.[28]

Results and Discussion

Phase Structural Determinations via SAXS Experiments in Reciprocal Space. After large-amplitude reciprocating shear, the diblock copolymer sample was oriented into a macroscopic "single-crystal"-like domain which was larger than the X-ray beam spot dimension. The 2D SAXS patterns along the three orthogonal directions (*x*, *y*, and *z* directions) have been shown in ref 26, which has been interpreted using a mixture of the trigonal ABC ($R\bar{3}m$) twins and the hexagonal AB ($P6_3/mmc$) structures. In this study, we used three-parameter (hkl) indices to describe both the trigonal and hexagonal cells. Note that one may also use a four-parameter index ($hkil$) to describe the hexagonal structure, where $i = -(h + k)$, and therefore, the $[uvtw]$ represents the lattice directions. In the (hkl) index system, the lattice directions adopt the $[UVW]$ system, where $U = 2h + k = u - t$, $V = h + 2k = v - t$, and $W = 1.5l(a/c)^2 = w$.[29] Here, the a and c are hexagonal unit cell dimensions. Therefore, in the $[UVW]$ system the [100], [120], and [001] directions of the hexagonal lattices for both the trigonal and hexagonal structures correspond to the *x*, *z*, and *y* directions in our PS-*b*-PEO sample (see Figure 2), respectively.

Since we have had 2D SAXS "single-crystal" patterns along the *x*, *y*, and *z* directions,[26] we could now use a tilting stage to obtain a series of tilted 2D SAXS patterns with different zones to quantitatively analyze the mixed HPL structures. If the initial position of the X-ray beam was parallel to the [001] direction and the sample was rotated along the [100]-axis (the *x*-axis) of the hexagonal lattices that include both the trigonal twins and hexagonal structure (see the schematic at the top of Figure 3), tilted diffraction patterns could be obtained. Figure 3a shows an example with the tilt angle $\theta = 39°$ (i.e., the X-ray is along the Z_1 direction in Figure 3), and the $[\bar{1}\bar{2}1]$ zone for the trigonal twins and the $[\bar{2}43]$-zone for the hexagonal structure were identified on the basis of the calculation. Upon superimposing these three calculated patterns, a mixed pattern was obtained. Every diffraction spot in the experimental pattern could be indexed when comparing this mixed pattern with the experimentally obtained diffraction pattern. When the θ increased to 58° (i.e., the X-ray is along the Z_2 direction in Figure 3), the $[\bar{2}\bar{4}1]$-zone for the trigonal twins and the $[\bar{4}83]$ zone for the hexagonal structure were obtained, and the results are shown in Figure 3b. Again, the three calculated patterns superimposed to represent the experimentally observed pattern. As one can see in these tilted patterns, all of the diffractions of the hexagonal structure superimposed with part of the diffractions of the trigonal twins, and the rest of the diffractions were entirely from the trigonal twins.

If we rotated the sample around the [120]-axis (the *z*-axis) of the hexagonal lattices, mixed patterns with different zones could also be identified. Figure 4a,b shows two examples. When the tilt angle (ϕ) was 35° as shown in Figure 4a (i.e., the X-ray is along the Z_3 direction in Figure 4), the [302] zone of the trigonal twins and the [101] zone of the hexagonal structure were observed. On the other hand, when the ϕ was 55° in Figure 3b (i.e., the X-ray is along the Z_4 direction in Figure 4), the [301] zone of the trigonal twins and the [201] zone of the hexagonal structure were obtained. All the diffractions in these patterns could be indexed. Although different from the tilt patterns obtained by rotating around the [100]-axis in Figure 3, most of the diffractions in Figure 4 were attributed to the hexagonal structure. Therefore, these patterns provide further evidence for the existence of the hexagonal structure in the HPL phase.

From these SAXS crystallographic analyses, the HPL was further confirmed as being a mixed phase with both trigonal twins and the hexagonal structure. Both lattices have the same in-plane unit cell parameters, $a_{tri} = a_{hex} = 26.6$ nm and $\alpha_{tri} = \alpha_{hex} = 120°$. Note that if a primitive unit cell is used for the trigonal twins, the unit cell parameters become $a_{tri} = b_{tri} = c_{tri} = 24.3$ nm and $\alpha_{tri} = \beta_{tri} = \gamma_{tri} = 66.3°$. The *c*-axes for the trigonal twins and the hexagonal structure were different: $c_{tri} = 56.7$ nm and $c_{hex} = 37.8$ nm. The c_{tri} is 1.5 times c_{hex}, because the trigonal twins contain three layers and the hexagonal phase contains two layers. One layer thickness was thus $d = c_{hex}/2 = c_{tri}/3 = 18.9$ nm. On the basis of the volume fraction of the PEO blocks (0.39) and TEM results (see below), the layer thicknesses for the PS and PEO blocks were 9.9 and 9.0 nm, respectively. The average diameter of the cylindrical PS perforations within the PEO layers was 12.2 nm. Nevertheless, their spatial arrangement needed to be examined using experimental observations in real space.

Visualization of "Plastic Deformation" via TEM Observations in Real Space. The formation mechanism of the HPL phase must be unique, in which the trigonal twins and the hexagonal structure have the

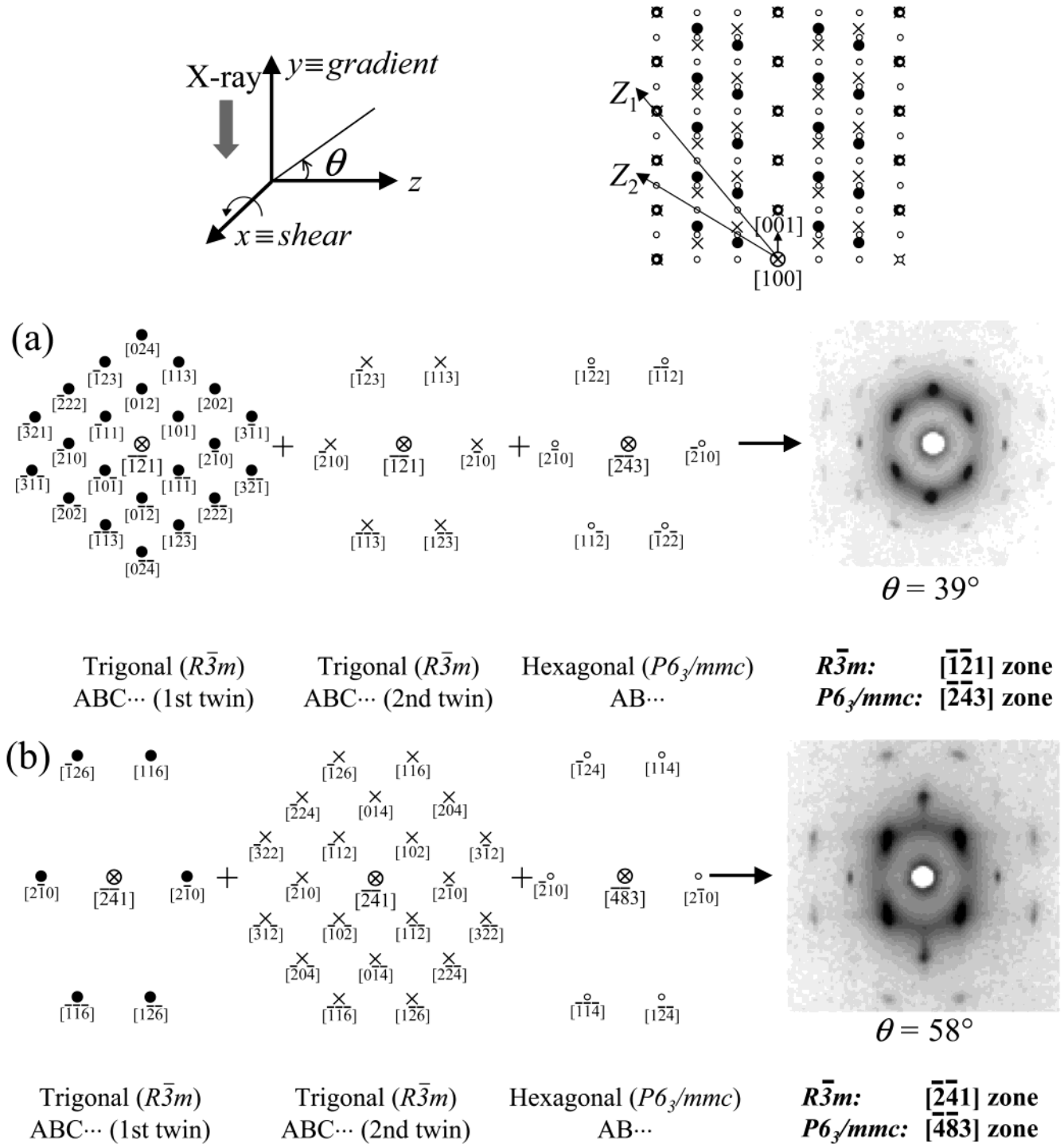

Figure 3. Interpretation of a tilt pattern when the tilt angle (θ) was (a) 39° and (b) 58°. As shown in the top, the tilting was along the [100] (the *x*-axis) direction and X-ray was coming from the top. The mixed diffraction pattern along the [100] direction[26] is shown on the top. The two tilt zones are indicated as Z_1 and Z_2.

identical in-plane "bond" and "orientational" orders. In other words, they are commensurate. The observed vertical streaks in the 2D SAXS patterns reported in Figure 1a of ref 26 suggest that these structures could be induced by various dislocations during mechanical shear, which is similar to the mechanical slips (plastic deformation) in metals.[30] To visualize the dislocations in real space, TEM experiments have been carried out. Bright-field TEM images along the [100], the [120], and the [001] directions are shown in Figure 5a−c. Note that the PEO microdomains appear darker in the TEM micrograph since the PEO blocks were easier to be oxidized (stained) by RuO_4 than the PS blocks.[27] From the 2D SAXS results, it is evident that the trigonal twins and the hexagonal structure could only be differentiated along the [100] (the *x*-axis) direction.[26] Therefore, the image to differentiate the trigonal ABC lattice and the hexagonal AB lattice is Figure 5a, which is viewed along the [100] direction. In this figure, the alternating perforated layers were oriented in the horizontal direction. At the bottom left part of Figures 5a, a trigonal lattice (ABC stacking) is shown (actually most of the area is the trigonal structure), while a small area of the hexagonal lattice (AB stacking) was observed in the top right. Figure 5b shows a rectangular arrangement of PEO microdomains with 2-fold symmetry. Defects could

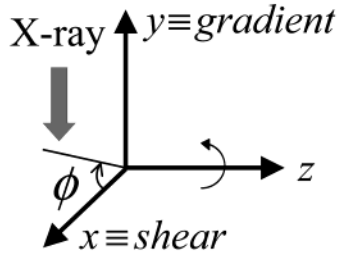

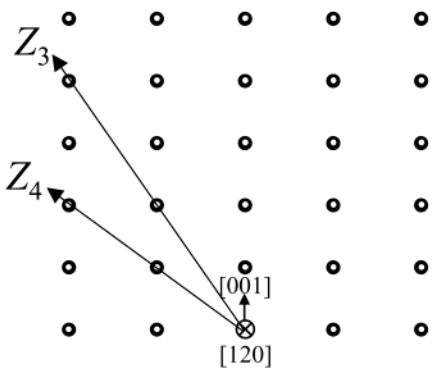

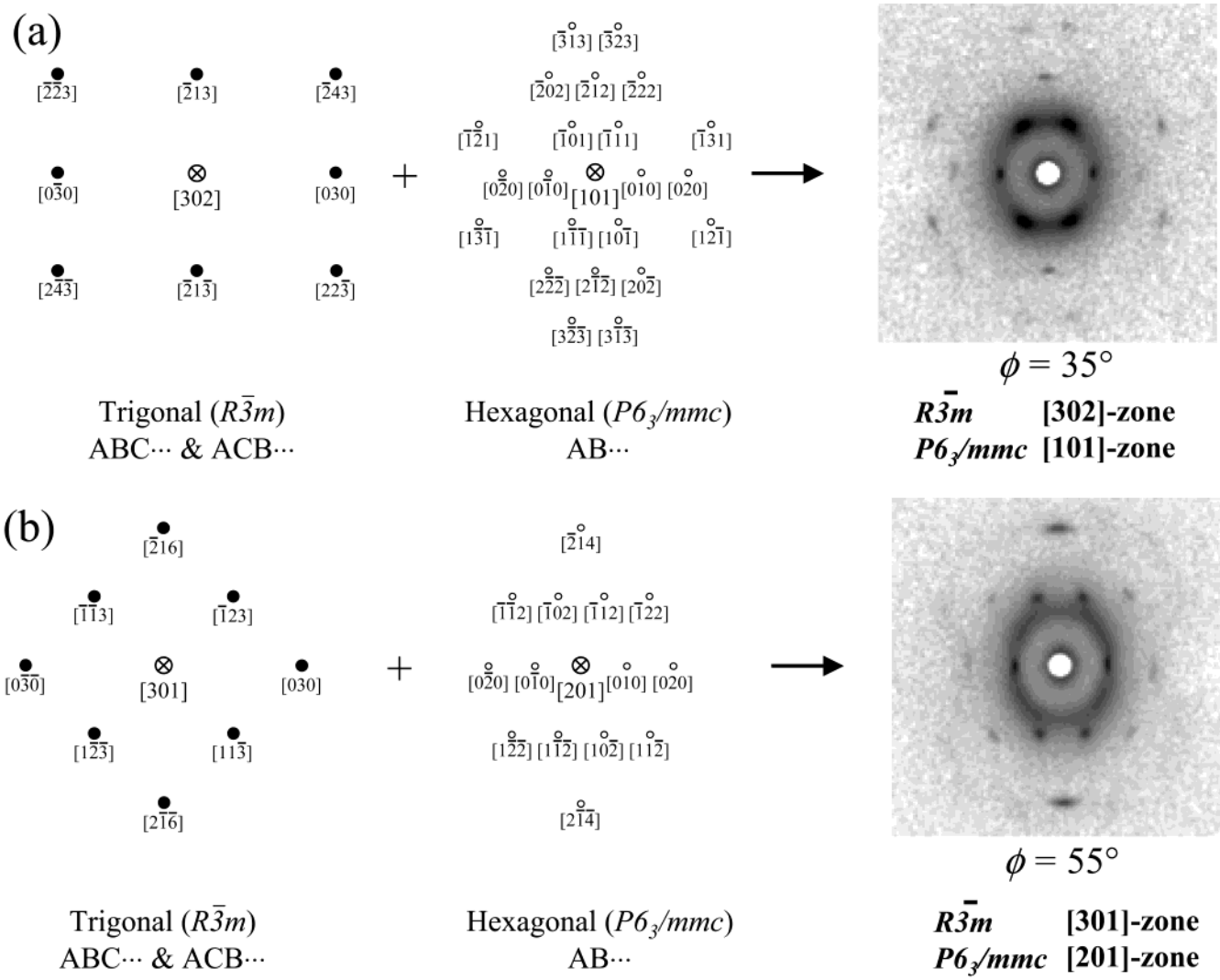

Figure 4. Interpretation of a tilt pattern when the tilt angle (ϕ) was (a) 35° and (b) 55°. As shown in the top, the tilting was along the [120] (the *y*-axis) direction and X-ray was coming from the top. The mixed diffraction pattern along the [120] direction[26] is shown on the top. The two tilt zones are indicated as Z_3 and Z_4.

be found in both figures (see below). Figure 5c illustrates white PS perforations within the dark PEO layers. The PS perforations arranging into a hexagonal lattice can be clearly seen from the micrograph inset at the lower corner.

In these figures, one can find several types of edge dislocations. The first and obvious type of edge dislocation is a *Frank partial dislocation* (see |− and −| symbols in Figure 5a,b) with a Burgers vector of $\mathbf{b}_F = c/3\langle 003\rangle$. A "vacancy loop" (absence of a layer) generates an intrinsic stacking fault, and an "interstitial loop" (inserting a layer) generates an extrinsic stacking fault. The second type is a *unit* (*perfect*) *dislocation* (see the ⊥ symbol in Figure 5a) having a $\{003\}\langle 100\rangle$ slip with a Burgers vector of $\mathbf{b}_U = a\langle 100\rangle$. The third and less obvious type is a *Shockley partial dislocation* with a Burgers vector, $\mathbf{b}_S = a/3\langle 120\rangle$. Any unit dislocation can be dissociated into two Shockley partial dislocations. Generally, one Shockley partial dislocation generates an intrinsic stacking fault, and two consecutive Shockley partial dislocations in the same direction generate an extrinsic stacking fault. The intrinsic and extrinsic

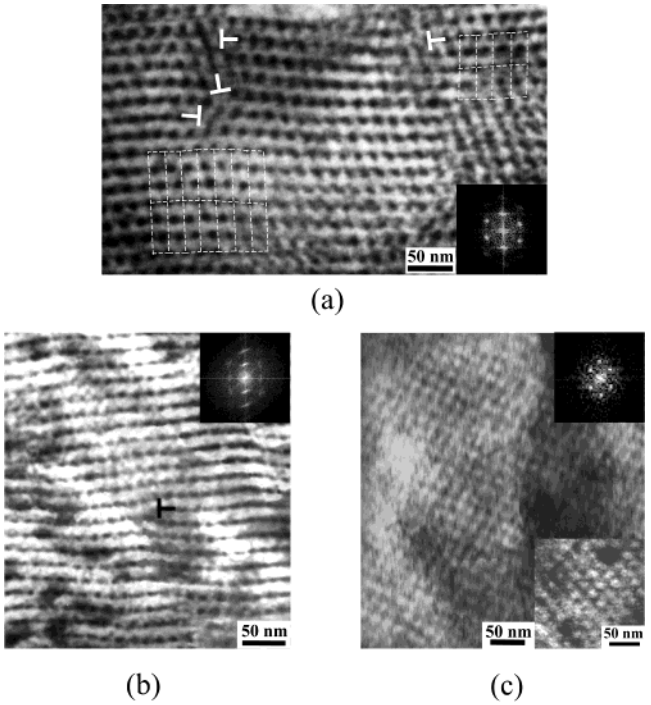

Figure 5. Bright-field TEM micrographs of a RuO_4-stained thin slices of the PS-*b*-PEO sample when the sectioning was perpendicular to (a) the [100] (the *x*-axis) direction, (b) the [120] (the *y*-axis) direction, and (c) the [001] (the *z*-axis) direction. The FFT results are shown as the insets.

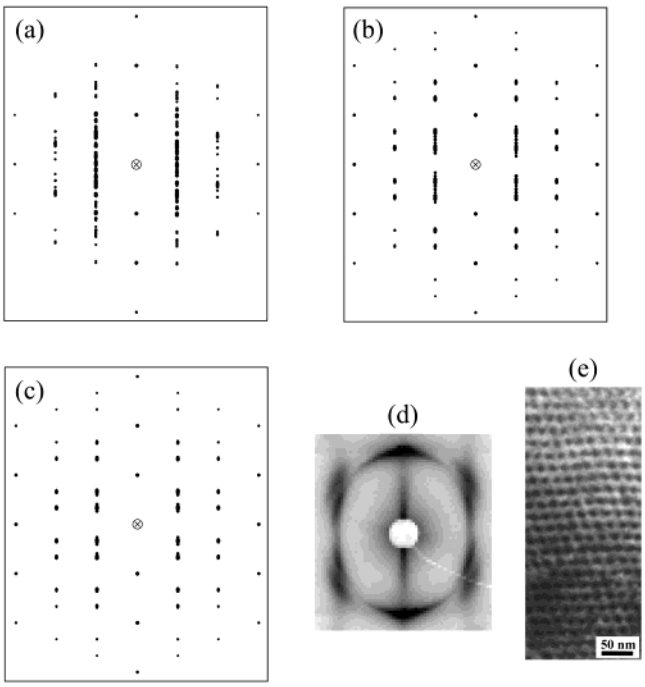

Figure 6. Computer-simulated diffraction results along the [100] direction (the *x*-axis) with (a) 30 random A, B, C layers in a supercell. (b) A twinned structure with 15 layers of ABC and 15 layers of ACB stacking sequences in a supercell. (c) A twinned structure with 21 layers of ABC and 21 layers of ACB stacking sequences in a supercell. (d) An enlarged diffraction area of the 2D SAXS pattern along the [100] direction (the *x*-axis). (e) A bright-field TEM micrograph showing 23-layer ABC stacking sequence.

stacking faults formed by either Frank or Shockley partial dislocations are geometrically equivalent. Detailed dislocation analysis can be found in ref 26. On the basis of these analyses, the formation mechanism for the trigonal twins has been attributed to successive intrinsic stacking faults on neighboring layers, while that for the hexagonal structure was attributed to successive intrinsic stacking faults on every second layer from a previous dislocation line (i.e., every third layer).

All these real space observations suggest that the origin of the twinning of trigonal lattices, and the formation of the hexagonal lattice was caused by "plastic deformation" due to these edge dislocations under large-amplitude mechanical shear, which is similar to that in imperfect metal crystals. The fast Fourier transformation (FFT) of the TEM micrograph in Figure 5a−c along the [100], [120], and [001] directions gave three diffraction patterns as shown in the insets of these figures. The diffraction pattern in the inset of Figure 5a resembles one of the trigonal twins (see Figure 3), since most of the area in Figure 5a was of the ABC stacking sequence. The FFT pattern inserted in Figure 5b fit the 2D SAXS pattern along the *z* direction (see Figure 4), while the inserted FFT pattern at the upper right in Figure 5c gave a 6-fold symmetry, indicating that the PS perforations arranged into a hexagonal lattice in the PEO layers.

Grain Sizes of the Trigonal Twins and the Hexagonal Structures along [001]. One question still remains: how do the trigonal twins and the hexagonal structure quantitatively arrange in the HPL phase? In other words, how often does the stacking fault occur in the sample? It is expected that the trigonal (003) twinning in the HPL phase could be polysynthetic (lamellar) twins, similar to those in minerals and metals.[31] However, the grain sizes for these trigonal twins and the hexagonal structure along the layer normal ([001]) direction were not known since no calibration of the Scherrer equation was available for SAXS analysis in this study. Ultrasmall-angle X-ray scattering has been used to estimate the average grain size in all directions for a lamellar styrene−butadiene diblock copolymer sample.[32] Here, as the fist step, we tried to obtain information about the specific correlation length along the [001] direction via computer-simulated SAXS pattern and TEM observations. Further investigations are required to extend this method to an ensemble-average method to introduce grain size distributions.

The SAXS experimental observation along the [100] direction exhibited streaks along the vertical ([001]) direction (see Figure 1a in ref 26). Therefore, we used computer simulations to evaluate the grain size along the [001] direction, and the simulated diffraction patterns are shown in Figure 6. Figure 6a is a simulated diffraction pattern of a super cell containing 30 layers of randomly stacked A, B, and C layers. One can see that the layer diffractions on the meridian were sharp, but the neighboring parallel layers in the quadrants had heavy streaks along the [001] direction, indicating disorder in the correlation between different layers. The simulated diffraction pattern of a super cell containing a twinned structure with 15 layers of an ABC sequence and 15 layers of an ACB sequence is shown in Figure 6b. In this figure, the vertical streaks become less prominent. However, the (011) and (012) diffractions of the trigonal twins still overlapped. When the ABC and ACB sequences increased to 21 layers in the twinned supercell, the simulated diffraction pattern showed discrete 011 and 012 diffractions (Figure 6c). This pattern was close to the experimental pattern as shown

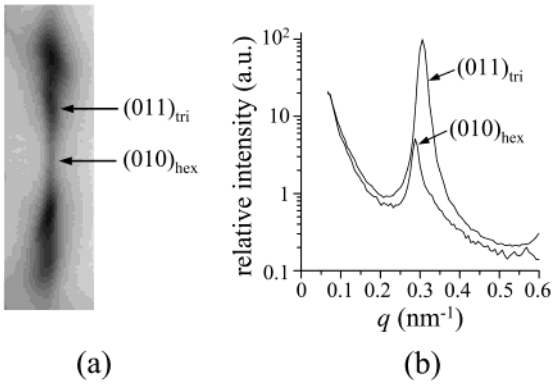

Figure 7. (a) Enlarged diffraction area in Figure 1a in ref 26 showing a $(010)_{hex}$ streak. (b) SAXS intensity profiles of the $(010)_{hex}$ and $(011)_{tri}$ reflections as shown in (a).

in Figure 6d. TEM studies also revealed ABC stacking with coherence over 20 layers, and an example having 23 layers of ABC stacking is shown in Figure 6e. Therefore, the grain sizes for the trigonal structure along the [001] direction should be relatively large (≥∼400 nm). Similarly, the correlation length for the hexagonal structure along the layer normal could also be evaluated from the streaking of the (010) diffraction of the hexagonal structure (Figure 7a and discussion below). We found that the correlation length for the hexagonal structure was relatively small.

To determine the relative population of both the trigonal twins and hexagonal structure, we needed to further analyze the intensity profiles of the $(010)_{hex}$ and $(011)_{tri}$ diffractions in Figure 1a of ref 26. An enlarged area of the $(010)_{hex}$ and $(011)_{tri}$ diffraction pattern is shown in Figure 7a. It is clear that the streak was along the vertical direction. The disorder between different layers could be introduced by a random arrangement of AB, AC, and/or BC stacking sequences. From the pattern in Figure 7a, the intensity profiles of the $(010)_{hex}$ and $(011)_{tri}$ diffractions with respect to q are shown in Figure 7b. The intensity of the $(011)_{tri}$ diffraction was about 20 times higher than that of the $(010)_{hex}$ diffraction. Computer-simulated diffraction intensities (structural factors) for the $(010)_{hex}$ and $(011)_{tri}$ diffractions in pure hexagonal and trigonal single-crystal diffraction patterns possessed a ratio of $I_{(011)tri}/I_{(010)hex} = 8.25$. A simple and approximate evaluation indicated that the population of the trigonal twins was around 80%, and the hexagonal structure composed about 20%. Note that in the evaluation we have to take into account the fact that the hexagonal structure contained two layers and the trigonal structure had three layers.

Metastability of the HPL Phase and Its Transformation Pathway toward the DG Phase. It has been demonstrated that the HPL phase was controlled by dislocations formed under dynamic mechanical deformation. We speculate that the relative population of the trigonal twins and the hexagonal structure may be dependent upon the shear amplitude and frequency. Therefore, the HPL phase should show a kinetics dependence. Rheological experiments were carried out to study the metastability of the HPL phase, and the results are shown in Figure 8. The first procedure involved a 100% amplitude and 1 rad/s frequency shear at 100 °C for 30 min on the sample to generate the HPL phase, as confirmed by SAXS experiments. The sample was subjected to a heating experiment under normal conditions in rheological tests of 1% amplitude/0.5 rad/s, as shown in the first run in Figure 8. The shear storage modulus G' first decreased with temperature and then began to increase at 148 °C. A maximum of the G' occurred at around 160 °C, representing an order-to-order transition. After this maximum, the G' values decreased continuously. As soon as the sample reached 200 °C, it was cooled to 100 °C under the same experimental conditions as in the first heating run in Figure 8. No order-to-order transition could be identified during this cooling experiment. Figure 8 also shows the second heating experiments under the same experimental conditions, and it overlaps with the previous cooling curve. The order-to-order transition was not found on this ramp, but the T_{ODT} was observed around 210 °C. The SAXS results of the ordered phase at 180 °C after the order-to-order transition are shown in Figure 9. The orientation in the sample was lost at high temperatures, as shown in the 2D SAXS pattern (the inset of Figure 9). The q ratio obeyed a rule of $\sqrt{6}:\sqrt{8}:\sqrt{14}:\sqrt{16}:\sqrt{20}:\sqrt{22}:\sqrt{24}:\sqrt{26}:...:\sqrt{50}$. This clearly suggests that the new phase formed at high temperatures had a double gyroid structure.[4,14] This indicates that during the cooling and

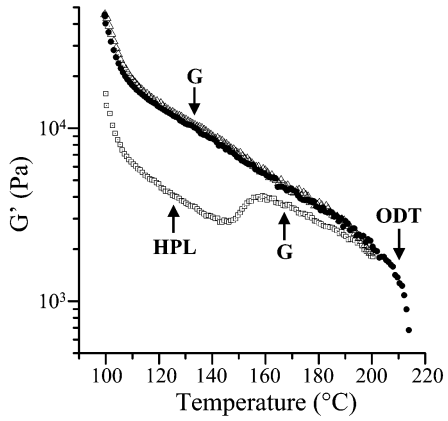

Figure 8. Low-frequency rheological measurements of shear storage modulus (G') on the PS-*b*-PEO diblock copolymer sample. The sample was presheared with 100% amplitude and 1 rad/s frequency at 100 °C for 30 min to induce the HPL phase. The open square symbols represent the first heating run. The open triangle symbols represent the first cooling run. The solid circular symbols are the second heating run.

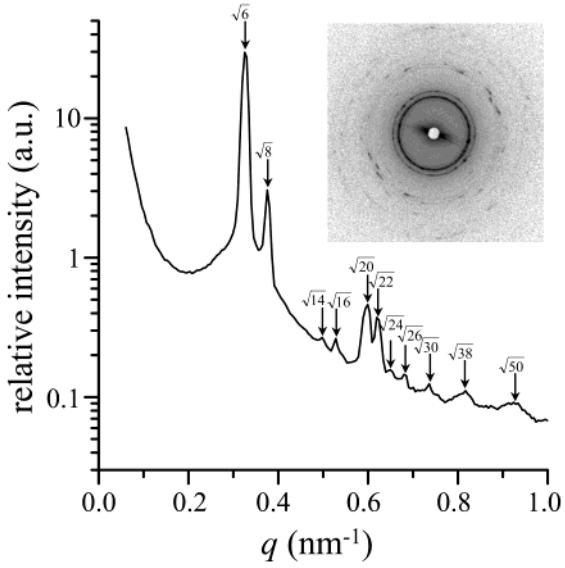

Figure 9. A 1D SAXS pattern of the double gyroid phase at a high temperature (180 °C) obtained by azimuthally integrating the entire 2θ angle region in the inset 2D SAXS pattern.

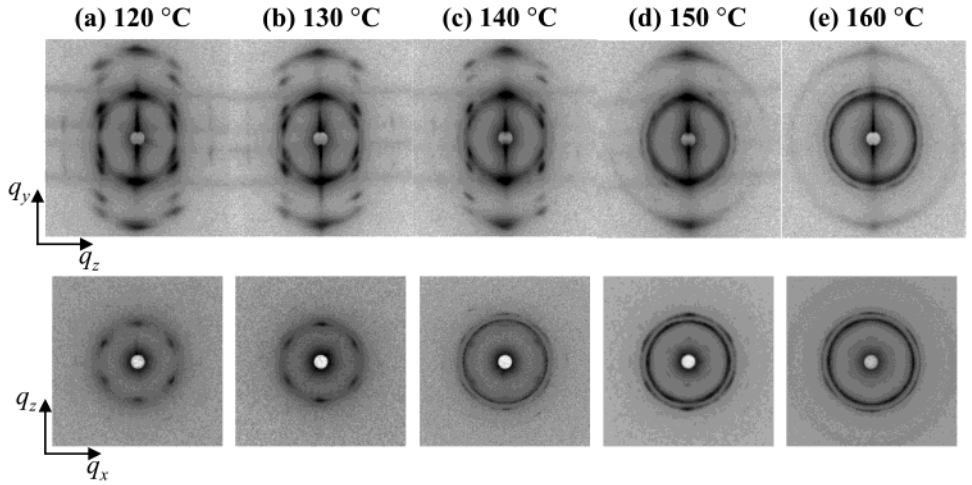

Figure 10. 2D SAXS patterns along the [100] (top) and [001] (bottom) directions for the HPL samples annealed at (a) 120, (b) 130, (c) 140, (d) 150, and (e) 160 °C for 15 min.

reheating processes the DG phase was retained in the entire temperature range studied. From the rheology measurement, the G' of the DG phase was higher than that of the HPL phase because the DG phase had a 3D bicontinuous structure and the HPL phase had a monocontinuous layer structure. If the sample was again subjected to large-amplitude shear at 100 °C, the HPL phase reappeared. Therefore, it could be concluded that the HPL phase was a long-lived metastable phase with respect to the DG phase, which is consistent with previous experimental findings.[25]

It has been observed that the HPL phase was in the weak segregation region of PS-*b*-PEO, and it could be transformed to the DG phase upon heating.[25,33] To understand the pathway of the transformation from the HPL phase to the DG phase in this diblock copolymer, a series of 2D SAXS experiments of the HPL samples annealed at different temperatures were carried out, and the results are shown in Figure 10. Since most of the information on structural changes was along the [100] (the *x*) and the [001] (the *y*) directions, we have only included the 2D SAXS patterns obtained along these two directions in Figure 10. After the sample was annealed at 120 °C, the SAXS patterns along all three directions were identical with those obtained at room temperature reported previously.[26] As shown in Figure 10a, both the trigonal (observed mainly along the [100] direction) and the hexagonal (the most inner 6-fold diffractions observed along the [001] direction) diffractions were identified.[26] When the annealing temperature increased to 130 °C (Figure 10b), the changes in diffraction intensities of the trigonal were different from those of the hexagonal structures. The trigonal (011), (012), (014), and (015) diffractions became more discrete than those in the 2D SAXS pattern along the [100] direction for 120 °C. Also, the hexagonal (100) diffractions in the [001] direction started to smear.

More visible changes of these patterns began at the annealing temperature of 140 °C as shown in Figure 10c. The intensity of the hexagonal (100) diffractions dramatically decreased as shown in the 2D SAXS pattern along the [001] direction. When the X-ray was along the [100] direction, the trigonal (011), (012), (014), and (015) diffractions sharpened, indicating that the HPL structure started to have internal rearrangements including further perfection of the lattices. This suggested that the hexagonal phase, which had a relatively short correlation length and was sandwiched between trigonal phases, probably rearranged its stacking sequence to become the trigonal phase during annealing since the hexagonal phase was less stable because it contained more stacking faults compared with the trigonal twins.[26] Therefore, the correlation length of the trigonal phase increased after the "annihilation" of the hexagonal structure, and the trigonal twin reflections became sharper when viewed along the [100] direction. However, a new phase was generated as evidenced from the 2D SAXS pattern along the [001] direction. The q values possess a ratio of $\sqrt{6}$:$\sqrt{8}$, indicating the development of a DG phase. The $\sqrt{6}$ diffraction was attributed to the {211} planes, and the $\sqrt{8}$ diffraction represented the {220} planes of the DG phase. Although the diffractions of the DG phase became less oriented, close inspection of the diffraction intensities revealed that certain orientations, in particular the $(220)_{DG}$ diffractions, showed a 6-fold symmetry that was identical to the (100) diffractions of the hexagonal structure. Azimuthal scan results of the $(211)_{DG}$ diffraction showed that this diffraction was along the [120] (the *x*) direction of the HPL structure. These observations indicate that the $[001]_{HPL}$ was coincident with the $[111]_{DG}$. Therefore, the epitaxy relationships for the HPL → DG transformation could be recognized as the $[100]_{HPL} \rightarrow [11\bar{2}]_{DG}$, the $[120]_{HPL} \rightarrow [\bar{2}20]_{DG}$, and the $[001]_{HPL} \rightarrow [111]_{DG}$, which were similar to those reported previously.[25,33]

When the annealing temperature was further increased to 150 °C, the layer diffractions remained, while all the quadrant trigonal diffractions disappeared when the X-ray was along the [100] direction. The (211) and (220) reflections of the DG phase became evident. This indicates that the perforations in the HPL phase started their rearrangement prior to the layer structure, and the correlations among the perforations in different layers started to be lost. The 2D SAXS pattern along the [001] direction showed no diffractions from the hexagonally arranged PS perforations and only the (211) and (220) diffractions of the DG phase. It was speculated that the thermal fluctuation was substantial and destroyed the correlations of the PS perforations in the PEO layers. The 6-fold symmetry for the (211) and (220) diffractions of the DG phase became dominant, indicating the epitaxy relationship of the $[001]_{HPL} \rightarrow [111]_{DG}$.

At the annealing temperature of 160 °C, which was within the HPL → DG phase transition region, the

SAXS patterns along the [100] direction showed the smeared $(211)_{DG}$ and the $(220)_{DG}$ diffractions. However, there were still discernible layer diffractions from the rearranged HPL phase with a q ratio of 1:2 on the meridian. The SAXS pattern along the [001] direction is typical of the DG phase along the $[111]_{DG}$ direction with smeared diffraction arcs.

These 2D SAXS results reveal that, during the transformation of the HPL → DG phase, the PS perforations in the hexagonal structure rearranged themselves first. The PS perforations in the trigonal twins of the HPL phase then joined the rearrangements at higher temperatures, while the layer features of the HPL phase were always kept. Only in the last step did the layer structure transform to the DG phase. It is speculated that the DG phase formation may nucleate from the perforation rearrangements. In the SAXS patterns, the d_{100}^{HPL} and d_{003}^{HPL} (layer thickness) are close to the d_{211}^{DG}. We might expect that the closer these d-spacings are, the easier the phase transformation can be.[33] Further investigations on the perforations rearrangements at elevated temperature during the HPL → DG transformation are needed.

Conclusion

The HPL phase in a PS-*b*-PEO diblock copolymer has been further confirmed by SAXS and TEM experiments. Detailed crystallographic analyses revealed that the HPL phase had a mixed morphology with a majority of trigonal twins (∼80%) and a minority hexagonal structure (∼20%). The trigonal twins and the hexagonal structure had the same in-plane unit cell parameters (a and α) but different c-axis dimensions because the trigonal twins contained three layers and the hexagonal structure contained two layers. Computer-simulated diffraction and TEM studies suggested that the correlation length of the trigonal structure along the [001] direction was large, i.e., over 20 layers (≥∼400 nm), while that for the hexagonal structure was relatively small. The formation mechanism of the unique HPL phase was studied by TEM in real space along the [100], the [120], and the [001] directions, and it was found to be a result of "plastic deformation" under the large-amplitude mechanical shear. Low-frequency rheological experiments suggested that the HPL phase was metastable, and it transformed into a more stable DG phase when the temperature exceeded 160 °C. However, the HPL phase could be regenerated if the sample was subjected the large-amplitude mechanical shear above the T_g^{PS} but sufficiently below the order-to-order transition temperature. Furthermore, the transformation from the HPL phase to DG phase was also systematically studied. The perforations of the hexagonal structure rearranged themselves first, followed by the perforations in the trigonal structure. The layers in the HPL phase were kept until the later stage in the development of the DG phase.

Acknowledgment. This work was supported by NSF (DMR-0203994) and University of Connecticut Research Foundation. The 2D SAXS experiments were carried out at the National Synchrotron Light Source at Brookhaven National Laboratory supported by the Department of Energy (DOE).

References and Notes

(1) Bates, F. S.; Fredrickson, G. H. *Annu. Rev. Phys. Chem.* **1990**, *41*, 525.
(2) Fredrickson, G. H.; Bates, F. S. *Annu. Rev. Mater. Sci.* **1996**, *26*, 501.
(3) Schulz, M. F.; Bates, F. S.; Almdal, K.; Mortensen, K. *Phys. Rev. Lett.* **1994**, *73*, 86.
(4) Hajduk, D. A.; Harper, P. E.; Gruner, S. M.; Kim, C. C.; Thomas, E. L.; Fetters, L. J. *Macromolecules* **1994**, *27*, 4063.
(5) Luzzati, V.; Spegt, P. A. *Nature (London)* **1967**, *215*, 701.
(6) Matsen, M. W.; Schick, M. *Macromolecules* **1994**, *27*, 7157.
(7) Matsen, M. W.; Bates, F. S. *J. Chem. Phys.* **1997**, *106*, 2436.
(8) Thomas, E. L.; Anderson, D. M.; Henkee, C. S.; Hoffman, D. *Nature (London)* **1988**, *334*, 598.
(9) Spontak, R. J.; Smith, S. D.; Ashraf, A. *Macromolecules* **1993**, *26*, 956.
(10) Disko, M. M.; Liang, K. S.; Behal, S. K.; Roe, R. J.; Jeon, K. J. *Macromolecules* **1993**, *26*, 2983.
(11) Almdal, K.; Koppi, K. A.; Bates, F. S.; Mortensen, K. *Macromolecules* **1992**, *25*, 1743.
(12) Hamley, I. W.; Koppi, K. A.; Rosedale, J. H.; Bates, F. S.; Almdal, K.; Mortensen, K. *Macromolecules* **1993**, *26*, 5959.
(13) Förster, S.; Khandpur, A. K.; Zhao, J.; Bates, F. S.; Hamley, I. W.; Ryan, A.; Bras, W. *Macromolecules* **1994**, *27*, 6922.
(14) Vigild, M. E.; Almdal, K.; Mortensen, K.; Hamley, I. W.; Fairclough, J. P. A.; Ryan, A. J. *Macromolecules* **1998**, *31*, 5702.
(15) Ahn, J. H.; Zin, W. C. *Macromolecules* **2000**, *33*, 641.
(16) Fredrickson, G. H. *Macromolecules* **1991**, *24*, 3456.
(17) Olvera de la Cruz, M.; Mayes, A. M.; Swift, B. W. *Macromolecules* **1992**, *25*, 944.
(18) Hamley, I. W.; Bates, F. S. *J. Chem. Phys.* **1994**, *100*, 6813.
(19) Matsen, M. W.; Schick, M. *Macromolecules* **1994**, *27*, 7157.
(20) Laradji, M.; Shi, A. C.; Noolandi, J.; Desai, R. C. *Macromolecules* **1997**, *30*, 3242.
(21) Matsen, M. W.; Bates, F. S. *J. Chem. Phys.* **1997**, *106*, 2436.
(22) Qi, S.; Wang, Z.-G. *Phys. Rev. E* **1997**, *55*, 1682.
(23) Qi, S.; Wang, Z. G. *Macromolecules* **1997**, *30*, 4491.
(24) Olmsted, P. D.; Milner, S. T. *Macromolecules* **1998**, *31*, 4011.
(25) Hajduk, D. A.; Takenouchi, H.; Hillmyer, M. A.; Bates, F. S.; Vigild, M. E.; Almdal, K. *Macromolecules* **1997**, *30*, 3788.
(26) Zhu, L.; Huang, P.; Cheng, S. Z. D.; Ge, Q.; Quirk, R. P.; Thomas, E. L.; Lotz, B.; Wittmann, J.-C.; Hsiao, B. S.; Yeh, F.; Liu, L. *Phys. Rev. Lett.* **2001**, *86*, 6030.
(27) Zhu, L.; Cheng, S. Z. D.; Calhoun, B. H.; Ge, Q.; Quirk, R. P.; Thomas, E. L.; Hsiao, B. S.; Yeh, F.; Lotz, B. *Polymer* **2001**, *42*, 5829.
(28) Trent, J. S.; Scheinbeim, J. I.; Couchman, P. R. *Macromolecules* **1983**, *16*, 589.
(29) Hahn, T., Ed. *International Tables for Crystallography*; Kluwer Academic Publishers: Dordrecht, 1996.
(30) Hume-Rothery, W.; Smallman, R. E.; Haworth, C. W. *The Structure of Metals and Alloys*; The Institute of Metals: London, 1988.
(31) Reed-Hill, R. E., Hirth, J. P., Rogers, H. C., Eds. *Deformation Twinning*, Gordon and Breach: New York, 1964.
(32) Myers, R. T.; Cohen, R. E.; Bellare, A. *Macromolecules* **1999**, *32*, 2706.
(33) Hajduk, D. A.; Ho, R.-M.; Hillmyer, M. A.; Bates, F. S. *J. Phys. Chem. B* **1998**, *102*, 1356.

MA021718X